Construction and Building Materials 299 (2021) 123975

Contents lists available at ScienceDirect

Construction and Building Materials

journal homepage: www.elsevier.com/locate/conbuildmat

Investigating the manufacturing technology and durability of lime mortars from Amaiur Castle (Navarre, Spain): A chemical–mineralogical and physical study

Graciela Ponce-Antón [a,*], Anna Arizzi [b], Giuseppe Cultrone [b], Maria Cruz Zuluaga [a], Luis Angel Ortega [a], Juantxo Agirre Mauleon [c]

[a] Department of Geology, Faculty of Science and Technology, University of the Basque Country-UPV/EHU, Sarriena s/n, 48940 Leioa, Bizkaia, Spain
[b] Department of Mineralogy and Petrology, Faculty of Sciences, University of Granada, Avda. Fuentenueva s/n, 18002 Granada, Spain
[c] Aranzadi Society of Sciences, Zorroagagaina 11, 20014 Donostia-San Sebastián, Gipuzkoa, Spain

HIGHLIGHTS

- Mineralogical, chemical and physical characterizations to assess mortar durability.
- Mineralogical characterization to approach knowledge of mortar manufacturing.
- Hydrotalcite and hydromagnesite in the lime mortar binder favours mortar strength.
- Traditional hot-mixing method was used for mortar manufacture at Amaiur Castle.

ARTICLE INFO

Article history:
Received 10 May 2020
Received in revised form 11 June 2021
Accepted 12 June 2021

Keywords:
Lime mortar
Deterioration
Hot-mixing method
Hydric behaviour
Hydromagnesite
Hydrotalcite

ABSTRACT

Mineralogical, chemical and physical characterization of archaeological lime mortars from different structures at Amaiur Castle (Navarre, Spain) was accomplished in order to comprehend their durability. Mortars from the south-west of the 16th century filling and bastion, and the south-east mortars of the17th century bastion are the most susceptible to deterioration due to their textural features. The high porosity and water absorption capacity, the poor interconnection of pores and slow drying are the main factors contributing to deterioration of mortar at Amaiur Castle. The mineralogical study enabled an approach to the technological knowledge used in the lime mortar manufacturing process at Amaiur Castle. Hydrotalcite and hydromagnesite identified in the mortar binder support the use of the traditional hot-mixing method during mortar manufacturing. This work provides valuable references for the formulation of compatible repair mortars to ensure suitable conservation of the castle as well as of other ancient structures built with similar materials.

1. Introduction

Knowledge of the composition and behaviour of historic mortars has improved since the first studies at the end of the 19th century [1]. Chemical and mineralogical investigations on these materials have indeed increased since the approval of the Venice Charter in 1964 [2] and the foundation of the International Council on Monuments and Sites (ICOMOS) in 1975 [3].

The study of historic mortars is currently considered an essential step in a restoration project, as it can determine the compatibility of original and repair mortars and, at the same time, allows the durability of the latter to be estimated on site [3–5]. All this with the final aim of ensuring appropriate conservation actions for the survival of our architectural heritage. More specifically, a chemical–mineralogical characterization of historic mortars is needed to investigate the mortar manufacturing technology and, at the same time, to guarantee compositional compatibility of the repair mortar. Physical studies aimed at assessing the pore system of the original mortars and their hydric behaviour are also needed to comprehend their durability under the environmental conditions in the historic building [6–10].

* Corresponding author.
E-mail addresses: graciela.ponce@ehu.eus (G. Ponce-Antón), arizzina@ugr.es (A. Arizzi), cultrone@ugr.es (G. Cultrone), mcruz.zuluaga@ehu.eus (M.C. Zuluaga), luis.ortega@ehu.eus (L.A. Ortega), zuzendaritza@aranzadi.eus (J.A. Mauleon).

https://doi.org/10.1016/j.conbuildmat.2021.123975
0950-0618/

Mortars show a complex pore system as they consist of a porous matrix and aggregates with variable porosity [11]. In porous building materials, water constitutes a major degradation agent since its circulation and retention within the pore system gives rise to various deterioration processes (e.g. salt crystallisation, freezing-thawing phenomena, etc.) that lead, in some cases, to irreversible damage [12,13]. Therefore, studying the porosity and pore size distribution of mortars enables an understanding of how water circulation through the mortar will affect the final building conservation [14,15].

Factors such as relative humidity, rainfall and temperature affect mortar durability [16,17]. In this sense, it is possible to relate the Köppen-Geiger climate types with the deterioration potential according to the local thermal-hygrometric conditions to which mortars are exposed [18–20].

Geographically, Amaiur Castle is located in the Oceanic maritime west coast climate zone (Cfb in the Köppen-Geiger climate classification) [21,22]. Annual average relative humidity in the area of the castle is 83.4%, reaching values above 86% in some months. The average annual precipitation is around 2040 mm, with rainfall above 90 mm every month of the year and above 200 mm in the wettest months [23,24]. At a relative humidity between 65% and 95%, water vapour and liquid water coexist, leading to the continuous presence of water within the pore system [11]. Furthermore, besides moistening the mortar, the meteoric water could also incorporate soluble CO_2 and salts inside the pores. While dissolved CO_2 favours the partial dissolution of carbonates, the volume increase due to the crystallization of secondary carbonates and/or soluble salts within the pores creates mechanical stress that will contribute to mortar deterioration [25–27].

From the point of view of the manufacturing technology of mortars used in Amaiur Castle (Navarre, Spain), previous studies have pointed to the possible use of the traditional hot-mixing method [28]. This manufacturing method consists in mixing the quicklime (i.e. non-slaked lime) with the moist aggregates and then adding water, so that lime slaking takes place simultaneously with the mixing of the mortar, which is applied when the mixture is still hot [29,30]. In this way, storage problems on site are reduced since the quicklime is used as soon as it is produced [31,32]. Due to their low porosity and high cohesion between the matrix and the aggregate, hot-mixed mortars are particularly appropriate for damp and cold climates and show excellent workability. They were therefore frequently used for core filling and foundation works [29,31]. By carrying out chemical–mineralogical analyses and physical studies on the mortars from the castle, it will be possible to corroborate that this traditional method was used during construction of the castle.

The present study aims to assess the material manufacturing technology and durability of historical lime mortars from Amaiur Castle by combining chemical, mineralogical and physical studies with the evaluation of the environmental conditions to which the materials are exposed. This will ensure correct planning and implementation of specific conservative actions aimed at controlling the decay of the castle over time. At the same time, this research will enable the suitable design of restoration projects that require the replacement of historic materials from the castle with new compatible repair mortars.

2. Archaeological background

Amaiur Castle is located in the north of the Baztan valley (Navarre, Spain), a strategic emplacement during the Middle Ages as it allowed visual control of the pass across the Pyrenees (Fig. 1). The castle of Amaiur constituted the last bastion of the Navarrese resistance by supporters of Henry II, king of Navarre, against the conquest by Ferdinand II of Aragon. After the final defeat of the last Navarrese resistance in 1522, the castle was looted and burnt [33,34] and the ruins remained buried until the excavations carried out by archaeologists of Aranzadi Society of Sciences in the period between 2006 and 2018.

Archaeological work carried out in Amaiur Castle revealed an occupation period from the 13th to the 17th century, but the first written sources mentioning the castle date back to the 12th century. During the 16th and 17th centuries, the castle defences were largely remodelled because of the evolution of artillery in the 14th century. The castle was reinforced, giving rise to a circular bastion, new rounded structures were added and the medieval walls were thickened by filling the space between the 13th-14th and the 14th-15th century walls with lime mortar. In the 17th century, diamond-shaped structures were added, thus transforming the fortification into a *trace italienne* bastion [33,34]. In the General Archives of Simancas, the different repairs are documented, including a repair in the south-east structure of the 16th century bastion [35,36]. Excavations at Amaiur Castle began in 2006 and continue to the present day, though only the 13th-14th century wall has been restored.

The works and repairs carried out in the castle over time as a result of the conflicts in the region could represent additional complexity in the study of mortars.

3. Materials and methods

3.1. Materials

Fourteen samples of lime mortar were collected from different structures at Amaiur Castle. Two samples come from the 14th-15th century wall (labelled M2), two from the cistern (labelled AL) corresponding to the lunette and barrel vault base, four from the core filling of the 13th-14th and 14th-15th century walls (labelled R), four from the rounded structure of the 16th century bastion (named B1) and two from the diamond-shaped structure of the 17th century bastion (labelled B2) (Fig. 1 and Table 1). Thus, the sample code of, for example, CA-M2-1 indicates CA: Amaiur Castle; M2: sample taken from the 14th-15th century wall; 1: sample number. The numbering does not always follow a consecutive order because some of these samples have already been used in previous research. Careful sampling avoided repaired areas in previous modern restoration work to ensure the collection of original historical mortars [28,37].

3.2. Methods

3.2.1. Mineralogical and textural characterisation

The mineralogy of mortars was determined by X-ray diffraction (XRD) on a powder sample using a Philips X'Pert diffractometer (Malvern PANalytical, Almelo, The Netherlands) equipped with a monochromatic Cu-$k_{\alpha 1}$ X-radiation (λ = 1.5405 Å) operating at 40 kV and 20 mA analysis conditions. The data collection was performed by a continuous scanning angle in the range from 5° to 70° 2θ and 0.02° s^{-1} goniometer speed. Mineral phase identifications were performed with X'Pert HighScore Plus 3.0 software (Malvern PANalytical, Almelo, The Netherlands) using the experimental patterns of ICDD and ICSD diffraction databases.

The microtexture and mineralogical nature of mortar components were determined on polished thin-sections using a Nikon Eclipse LV100POL optical polarizing microscope equipped with DS F-I1 digital camera and a DS L-2 control unit in both transmitted and reflected polarized light modes. A comparison chart for visual percentage estimation was used to define the mortar binder/aggregate ratios [38].

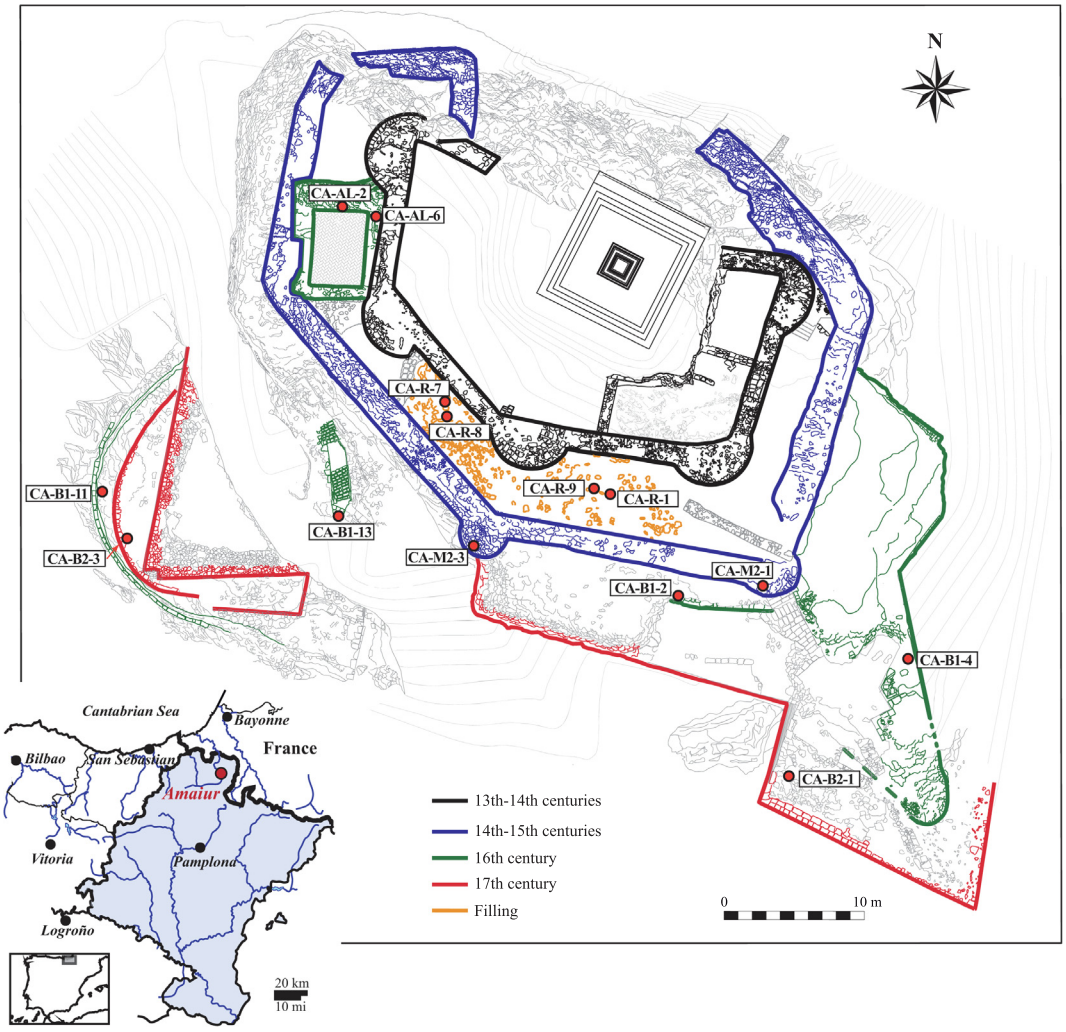

Fig. 1. Geographic location of Amaiur Castle (Navarre, Spain) and the plan of the castle with the sample locations marked by red circles. Modification from Ponce-Antón et al. (2020). (For interpretation of the references to colour in this figure legend, the reader is referred to the web version of this article.)

Table 1
Studied mortar samples taken from the different structures at Amaiur Castle. * Lunette; **Barrel vault base; #Structure foundation. In grey the samples located in the SE of the Castle. (Sample Code is described in the text.)

Chronology	14th-15th centuries	1512-1522			1635
Archaeological Structure	Wall	Cistern	Core filling	16th Bastion	17th Bastion
Samples	CA-M2-1	CA-AL-2 *	CA-R-1	CA-B1-2	CA-B2-1
			CA-R-9	CA-B1-4	
	CA-M2-3	CA-AL-6 **	CA-R-7	CA-B1-11 #	CA-B2-3 #
			CA-R-8	CA-B1-13	

3.2.2. Chemical characterisation

Elemental chemical composition of major elements of mortars was determined by means of X-ray Fluorescence (XRF) using a Wavelength Dispersive X-ray Fluorescence (WDXRF) PANalytical Axios Advanced PW4400 XRF spectrometer with 4 kW Rh anode SST-mAX X-ray tube with a detection limit of 0.01 wt%. Fused beads were obtained by melting the powder bulk mortar sample with lithium borate flux (Spectromelt A12, Merck) in 20:1 proportion at 1200 °C for 3 min in Pt/Au crucibles using a PANalytical Perl'X3. The loss on ignition (LOI) was calculated after heating the powder bulk mortar sample at 1050 °C for one hour.

3.2.3. Study of pore system and hydric behaviour

The pore size distribution (PSD) and the open porosity (P_{MIP}) were determined by mercury intrusion porosimetry (MIP) using a Poremaster-60 GT porosimeter (Quantachrome Instruments), with a maximum injection pressure of 414 MPa, measuring the pore diameter in a range of 0.003 to 360 μm. Mortar fragments of ca. 1 cm^3 were oven-dried for 24 h at 60 °C and then analysed. MIP analysis could not be performed in all samples due to the scarcity of the archaeological material.

Hydric tests (HT) were carried out to complete the study of the pore system and to assess the parameters associated with fluid uptake and circulation through the pore system. Measurements were performed under controlled thermo-hygrometric conditions at 25 °C and 50% relative humidity at atmospheric pressure on mortar samples of 3 cm^3 previously oven-dried at 80 °C for 24 h. Due to the archaeological nature of the samples, hydric tests were performed on no more than two or three samples per mortar type. The free water absorption (A_b), forced water absorption (A_f, under vacuum) and absorption coefficient (C_a) were calculated following the UNE-EN 13,755 [39] standard. The degree of pore interconnection (A_x) [40] and the saturation coefficient (S) [41] were also calculated. UNE-EN 1936 [42] standard was used to determine the open porosity (P_{HT}) and skeletal ($>_{Hsk}$) and bulk ($>_{Hb}$) densities. Drying index (D_i) was determined according to the NORMAL

29/88 [43]. The capillarity coefficient (C_c) and the capillarity height (H_c) were determined according to the UNE-EN 1925 [44] standard.

3.2.4. Non-destructive tests

Ultrasonic pulse velocity tests provide an indirect assessment of the textural features of mortars (e.g. porosity, anisotropies, etc.) [45]. Propagation velocity of ultrasonic pulses was measured using a Controls 58-E4800 ultrasonic pulse velocity tester with non-polarised piezoelectric transducers of 54 MHz. A viscoelastic couplant gel (Transonic gel) was used to ensure proper contact between the transducers and the surface of the mortar sample. Measurements were performed under controlled thermo-hygrometric conditions at 25 °C and relative humidity of 50% on samples 3 cm^3 in size previously oven-dried at 80 °C for 24 h. The test was performed on two or three samples per mortar type. The propagation velocity of P waves (V_p) was calculated according to the ASTM D 2845-05 [46] standard and the V_p values were used to calculate the structural anisotropy (ΔM) [47].

The aesthetic compatibility between a repair mortar and the original one is another important requirement to be fulfilled during restoration work [5,48]. With this in mind, the colour of samples was measured according to the CIELAB (CIE 1976 L*a*b*) colour space system proposed by the International Commission on Illumination (CIE) following the UNE-EN 15886 [49] standard. The lightness (L*) and chromatic (a* and b*) parameters were obtained using a Konica-Minolta CM-700d portable spectrophotometer on an area 8 mm in diameter, 10° view angle, D65 standard illuminant, with SCI/SCE modes and 400–700 nm wavelength range. Colour measurements were performed in five different points of each mortar sample and the mean value was calculated.

4. Results and discussion

4.1. Mineralogical, chemical and textural characterization

X-ray diffraction (XRD) results are given in Table 2 and the X-ray diffraction pattern of one of the most representative mortars (CA-M2-3) is shown in Fig. 2. All samples are mainly composed of magnesium calcite [$(Ca,Mg)CO_3$] and dolomite [$CaMg(CO_3)_2$] in different relative amounts. Quartz [SiO_2] was identified in minor amounts, particularly in samples from the cistern (samples CA-AL-2 and CA-AL-6) and the 17th century bastion (samples CA-B2-1 and CA-B2-3). Hydromagnesite [$(Mg_5(CO_3)_4(OH)_2{\cdot}4H_2O)$] and hydrotalcite [$Mg_6Al_2(CO_3)(OH)_{16}{\cdot}4(H_2O)$] were also detected.

Hydrotalcite formation is favoured during the lime-slaking process in the presence of Mg^{2+} and Al^{3+}, [50] and hydromagnesite formation is favoured during lime mortar carbonation under high humidity conditions and in the presence of available magnesium [51]. It is known that the presence of the Mg-phases contributes to the strength and durability of the magnesian mortars [52,53]. Presence of hydrotalcite in the mortar binder also constitutes a potential contaminant mineral for radiocarbon dating [50].

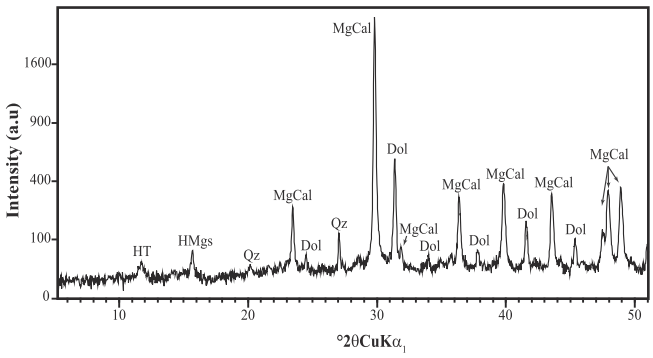

Fig. 2. The most representative X-ray diffraction pattern of the studied mortars, corresponding to Sample CA-M2-3. Dol: dolomite, HMgs: hydromagnesite, HT: hydrotalcite, Mg-Cal: magnesium calcite, Qz: quartz.

The chemical composition determined by X-ray fluorescence (XRF in Table 3) is in accordance with the mineral phases identified by XRD. The high CaO values (>30 wt%) measured in all samples are mainly related to the calcite. In contrast, the MgO content is related to the presence of different amounts of dolomite, hydromagnesite and hydrotalcite. The Si values are mainly linked to the presence of quartz in the samples; the higher values in samples CA-AL-2, CA-AL-6 and CA-M2-3 are noteworthy. Al values are related to the hydrotalcite but the presence of Fe, K and Ti indicates the presence of phyllosilicates and feldspars that were not detected by XRD as their amount is under the detection limit of the technique. High LOI values (>40 wt%) reflect the carbonated nature of the mineral phases of which mortars are mainly composed.

Macroscopically, all mortars show a heterogeneous texture in aggregate size, mainly of carbonated nature with angular to subangular shape (Fig. 3a-c). Sub-rounded ceramic fragments are also observed scattered in the matrix of all samples (Fig. 3d and e), with the largest fragments of up to 1 cm in size observed in mortars from both bastions (Fig. 3f). The fact that no hydraulic phases have been detected by XRD raises doubts about the deliberate purpose of achieving hydraulic properties in mortars with the addition of ceramic fragments.

Mortars from the fill stand out as they contain the highest aggregate content and largest aggregate grains, which reach >2 cm in size and are poorly graded. Nevertheless, the filling mortars from the south-east area (samples CA-R-1 and CA-R-9) show fewer aggregates than those from the south-west area (samples CA-R-7 and CA-R-8) (Fig. 3g and h, respectively). In contrast, mortar samples from the lunette and barrel vault base of the cistern (samples CA-AL-2 and CA-AL-6, respectively) show the smallest amount of aggregates (Fig. 3i). Mineralogical nature, grading and shape of aggregates used in mortar manufacture also play an important role in the mechanical behaviour of mortar and therefore they are important characteristics to consider in repair mortar formulation [54]. In this regard, the angular carbonated aggregates with rough surface favour the nucleation of the calcitic binder and

Table 2
X-ray diffraction results for the bulk lime mortar from Amaiur Castle. MgCal: magnesium calcite, Dol: dolomite; Qz: quartz, HMgs: hydromagnesite, HT: hydrotalcite. The amount is expressed as: -: undetected, tr: trace; *: low proportion; **: medium proportion; ***: high proportion; ****: predominant phase.

	CA-M2-1	CA-M2-3	CA-AL-2	CA-AL-6	CA-R-1	CA-R-7	CA-R-8	CA-R-9	CA-B1-2	CA-B1-4	CA-B1-11	CA-B1-13	CA-B2-1	CA-B2-3
MgCal	****	****	****	***	***	****	****	***	***	***	***	****	****	***
Dol	**	**	**	***	***	**	**	***	**	***	**	**	**	**
Qz	tr	*	*	*	tr	tr	tr	tr	*	tr	tr	tr	*	*
HMgs	–	*	–	–	tr	*	–	tr	–	–	–	tr	–	–
HT	tr	*	*	tr	tr	*	–	*	tr	tr	–	tr	–	–

Table 3
X-ray fluorescence results of major elements in the bulk lime mortars from Amaiur Castle. Results are expressed as oxides in wt %. Iron content is expressed as total Fe_2O_3t. LOI: loss on ignition (%).

	CA-M2-1	CA-M2-3	CA-AL-2	CA-AL-6	CA-R-1	CA-R-7	CA-R-8	CA-R-9	CA-B1-2	CA-B1-4	CA-B1-11	CA-B1-13	CA-B2-1	CA-B2-3
SiO_2	3.27	4.29	4.56	4.34	2.57	2.24	3.89	3.42	3.43	3.45	2.22	2.25	2.33	3.39
Al_2O_3	1.13	1.73	1.67	1.42	0.93	0.95	1.06	0.89	1.44	1.53	0.88	0.76	0.55	1.27
Fe_2O_3t	0.73	0.92	0.81	0.70	0.77	0.77	0.81	0.80	0.81	0.66	0.58	0.70	0.56	0.67
MnO	0.02	0.02	0.02	0.01	0.02	0.02	0.02	0.03	0.02	0.01	0.01	0.03	0.01	0.02
MgO	11.58	10.86	8.03	9.14	14.07	13.58	8.40	15.07	11.79	8.36	5.86	11.85	8.85	9.85
CaO	37.04	36.90	37.74	38.57	34.15	33.72	39.88	33.00	35.98	37.51	43.41	36.70	41.93	37.09
Na_2O	0.08	0.01	0.03	0.02	0.05	0.02	0.02	0.03	0.05	0.04	0.03	0.00	0.01	0.05
K_2O	0.17	0.22	0.36	0.33	0.20	0.16	0.23	0.25	0.32	0.20	0.15	0.11	0.08	0.17
TiO_2	0.05	0.06	0.09	0.07	0.04	0.05	0.05	0.05	0.06	0.05	0.04	0.05	0.03	0.04
P_2O_5	0.02	0.01	0.02	0.04	0.01	0.02	0.04	0.02	0.02	0.01	0.02	0.02	0.01	0.03
SO_3	0.03	0.01	0.05	0.03	0.04	0.01	0.02	0.04	0.04	0.03	0.02	0.01	0.03	0.03
LOI	43.66	43.54	42.08	42.89	45.18	44.91	42.84	44.24	43.98	42.85	41.10	44.76	43.85	43.52

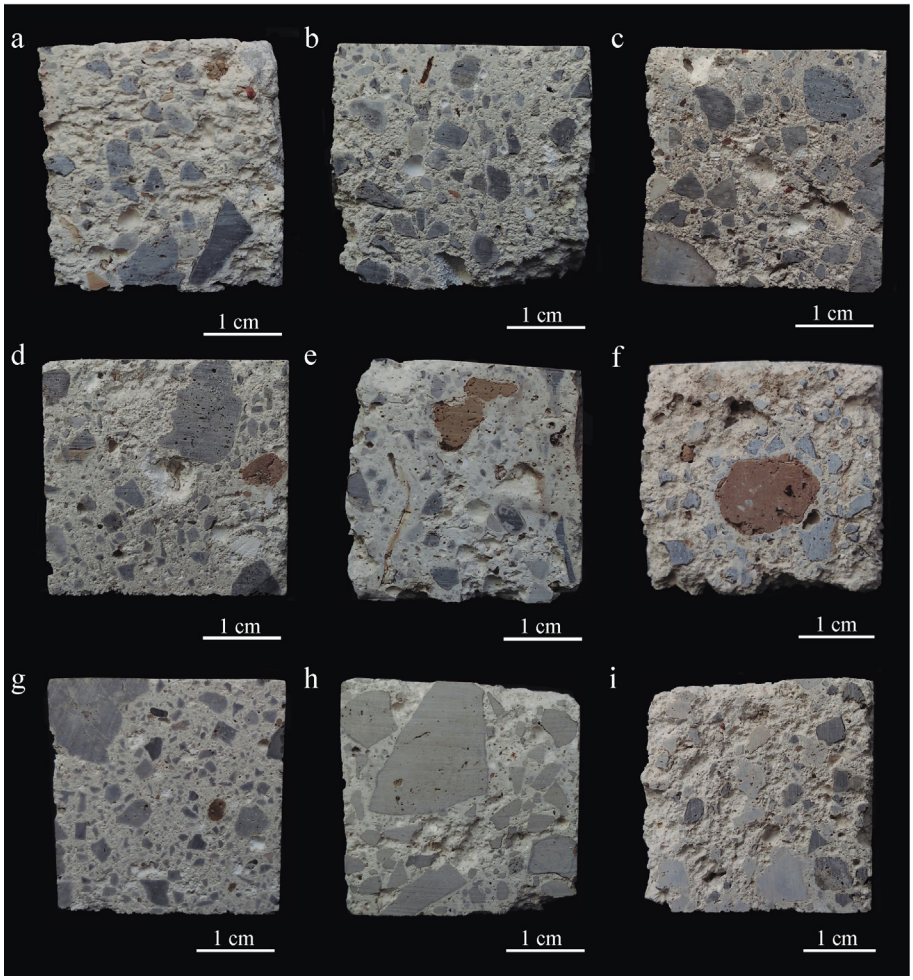

Fig. 3. Images of the most representative textures of the hand samples of Amaiur Castle lime mortars. (a-c) Mortars showing a representative heterogeneous texture with angular to subangular carbonated aggregates. (d-f) Different grain sizes of subrounded ceramic fragments. (g) Filling mortar sample from the SE area showing the highest amount of aggregates. (h) Filling mortar sample from the SW area showing the largest aggregates. (i) Mortar from the cistern showing the least amount of aggregates. (a) Sample CA-M2-1, (b) Sample CA-B1-2, (c) Sample CA-B1-13, (d) Sample CA-R-9, (e) Sample CA-M2-3, (f) Sample CA-B2-3, (g) Sample CA-R-1, (h) Sample CA-R-8, (i) Sample CA-AL-6.

a similar composition of the two components leads to better cohesion between the aggregates and binder, thus improving the mechanical strength of the mortar [55–58]. Moreover, the use of coarse aggregates in the manufacture of the filling mortar could have favoured the volume stability of the mixture, also improving long-term strength [59].

The petrographic study supported the macroscopic observations, allowing a better characterization of the microtextural features of mortars. Microscopically, all samples show a heterogeneous binder matrix-supported texture with a binder/aggregate ratio between 1:2 and 1:1. Carbonated aggregates are angular to subangular dolostone fragments embedded in a micritic

calcite matrix (Fig. 4a). The dolostone used as aggregates corresponds to the surrounding geological materials [60,61]. In addition to the subrounded ceramic fragments (Fig. 4b), some subrounded sandstone fragments up to 2.5 mm in size are also observed (Fig. 4c). Quartz grains up to 0.6 μm in size are observed dispersed in the matrix; the largest appeared in the samples from the 17th bastion. All samples show heterometric dolostone fragments ranging from 0.1 mm to 2.5 mm in size whereas those>5 mm were in the filling mortars (Fig. 4d). Lime lumps are also observed (Fig. 4e). Small dark spots are observed in the binder related to Mg-rich areas (Fig. 4f) from which the acicular hydromagnesite crystals grow. Hydromagnesite crystals have also been observed growing from the edge of pores (Fig. 4f and g). Petrographic observations are in accordance with X-ray diffraction results (Table 2).

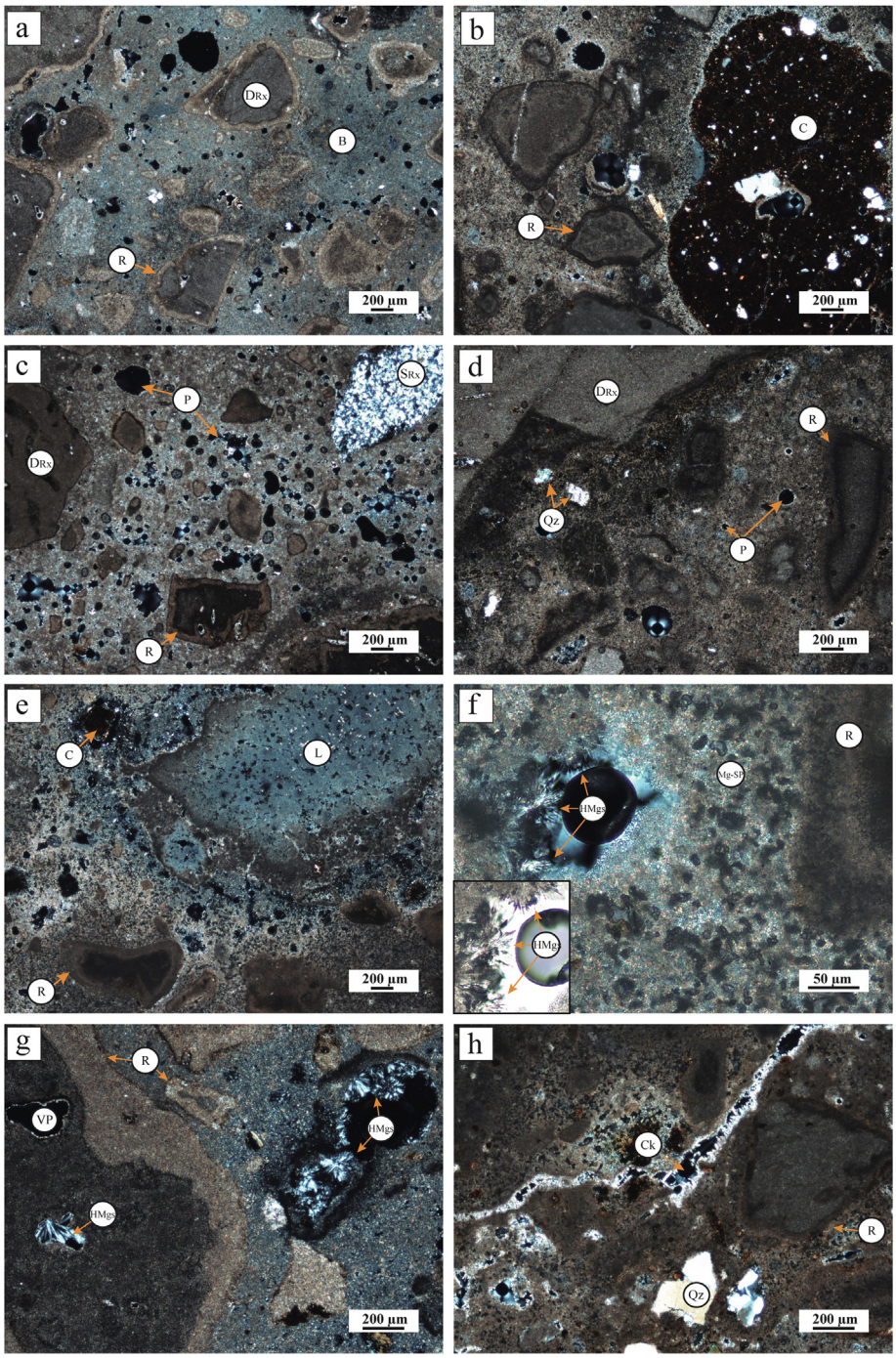

Fig. 4. Photomicrographs of the most representative microtextural features of the lime mortars from Amaiur Castle. (a) Heterogeneous binder matrix-supported texture with angular to subangular dolostone fragments embedded in a micritic calcite matrix. (b) Mortar with a subrounded ceramic fragment. (c) Sandstone aggregate in a mortar with high porosity. (d) Large dolostone aggregate in a mortar with low porosity. (e) Mortar with a lime lump. (f) Mortar with Mg-rich spots and hydromagnesite crystals. (g) Hydromagnesite crystals filling the binder pores and dolostone vuggy pores. (h) Microcracks with secondary calcite inside. Reaction zone in the dolomitic aggregates is seen in all photomicrographs. B: binder. C: ceramic fragment. SCal: secondary calcite. Ck: microcrack. DRx: dolostone. HMgs: hydromagnesite. L: lime lump. Mg-SP: Mg-rich spot. P: pore. Qz: quartz. R: reaction zone. SRx: sandstone. VP: vuggy porosity. (a) Sample CA-M2-1, (b) Sample CA-B1-2, (c) Sample CA-B1-4, (d) Sample CA-R-9, (e) Sample CA-AL-2, (f) Sample CA-R-1, (g) Sample CA-M2-3, (h) Sample CA-B1-11.

The presence of small hydromagnesite acicular crystals filling pores indicates that this Mg-phase was one of the last phases to crystallize. This is in agreement with the low Mg^{2+} and CO_3^{2-} concentrations needed for hydromagnesite crystallization [62]. The presence of hydromagnesite improves cohesion between binder and aggregates, favouring mortar strength [63].

Binder porosity is characterized by irregular-shaped pores bigger than 500 μm in size. Sample CA-B1-4 from the 16th century bastion stands out for its high porosity whereas the filling mortar samples from the SW area (samples CA-R-7 and CA-R-8) show the lowest porosity (Fig. 4c and d). Dolostone fragments are characterized by *vuggy* porosity (Fig. 4g). Microcracks filled with secondary calcite can also be observed in the binder-matrix of samples CA-AL-6, CA-B1-11 and CA-B2-3, and above all in sample CA-M2-1 (Fig. 4h).

Dolomitic aggregates stand out because of their pronounced reaction zone, which can be observed in all images in Fig. 4. According to Ponce-Antón et al. [28], the reaction zone in the dolostone fragments originated from the dedolomitization of dolomitic aggregates as a result of a portlandite-dolomite reaction. This phenomenon, together with the fact that hydrotalcite has been detected in the binder, suggests that a traditional hot-mixing method might have been used for the manufacture of the mortars at Amaiur Castle. According to Copsey [30], in the traditional hot-mixing method the quicklime (CaO) is slaked mixed with the aggregates, reaching temperatures of nearly 200 °C, and as water is added temperatures drop under 100 °C, to around 58 °C at the end of the slaking. However, these temperatures will depend on the slaking conditions.

Hydrotalcite formation has been described in mortars cured at 60 °C [64,65], and hydromagnesite requires temperatures over 50 °C to crystallize [62,66]. The observed white lumps are also characteristic of hot-mixed mortars [29].

The high Ca and Mg values measured by XRF are consistent with the calcite binder matrix-supported texture of mortar and the dolomitic nature of the aggregates. The K, Fe and Ti values are related to phyllosilicates, feldspars and oxides present in the ceramic fragments observed in the petrographic study, even if they were not detected by XRD (Table 2).

The dedolomitization of the dolomitic aggregates could add magnesium to the system, hindering the determination of the magnesium content in the lime used in the mixture. This input could have favoured the formation of Mg mineral phases detected by X-ray diffraction. Thus, the presence of magnesium could have made the mortar work as if it were made with dolomitic lime.

4.2. Characterization of pore system and hydric behaviour

Table 4 summarises the obtained mercury intrusion porosimetry (MIP) data. The highest porosity values (P_{MIP}) were measured in samples CA-B1-4 and CA-B2-3 (45% and 37.8%, respectively), whereas the lowest values were measured in sample CA-R-8 and sample CA-B1-13 (26.3% and 27.7%, respectively).

Regarding the pore size distribution (PSD) (Fig. 5), all samples show a family of small pores of $0.01 < r < 1$ μm connected to a family of large pores of $1 < r < 10$ μm, with a greater volume of pores of $0.1 < r < 1$ μm characteristic of the matrix of lime mortars [67,68]. Samples CA-B1-2 and CA-B2-1 are also characterized by a family of large pores of $10 < r < 100$ μm. The bimodal PSD with two main peaks situated at around 0.1 μm and at around 1 μm is shown by most samples, except for samples CA-M2-1 and CA-B2-3, which show a nearly unimodal pore size distribution with a main peak at around 1 μm. Samples CA-B1-4 and CA-B2-3 stand out not only for the highest P_{MIP} values but also for, respectively, a marked bimodal and unimodal pore size distribution (Fig. 5).

The family of smaller pores is related to the aggregate porosity, although some dolostone fragments show scarce larger pores, whereas the larger pore family is related to the binder porosity (Fig. 4).

Hydric tests (HT) were performed for a better study of the pore system and to evaluate the hydric behaviour of samples (Fig. 6 and Table 4) and therefore their susceptibility to deterioration.

The degree of pore interconnection values (A_x) was lower in samples CA-AL-2, CA-AL-6 and CA-B2-3 (<3%), indicating better pore interconnection that favours water flow through the mortar. In contrast, samples CA-R-8, CA-B1-11, CA-B1-13 and CA-B2-1 show the highest A_x values (>9%), which indicates greater difficulty of water to flow due to worse pore interconnection. Considering the lowest A_x values of the samples from each structure (Table 4), sample CA-AL-6, sample CA-M2-3 (from the south-west) and samples CA-R-1, CA-B1-2, CA-B1-4 and CA-B2-3 (from the south-east) show the lowest A_x values. Samples with better pore interconnection are those that display a higher saturation coefficient (S), since S values are related to the A_x parameter.

Regarding the drying curve, at the beginning of the test the drying rate is constant. Curves closer to the vertical correspond to samples that dry faster (Fig. 6a). Once the critical moisture content is reached, the drying rate decreases, and pore size and pore interconnection are the factors controlling the drying velocity [69]. Samples with the highest drying index values ($D_i > 0.248$) dry more slowly and the porous system remains full of water for longer. Samples CA-R-1 and CA-R-9 stand out for taking the longest to dry ($D_i = 0.251$) and sample CA-B1-4 for drying the fastest ($D_i = 0.240$).

Capillary uptake curves (Fig. 6b) show the typical capillary rise trend for lime mortars characterized by two different slopes [70,71]. The first sharp slope is related to rapid water absorption at the beginning of the test. From 24 h of the test, the absorption velocity decreased and the water uptake became slow and continuous leading to a more linear slope until saturation at 250 h. The capillary front of all samples also reached a peak after 24 h (Fig. 6c). The two slopes in the capillary uptake curve and the time-lag between visual and real saturation confirms the two main pore families ($0.01 < r < 1$ μm and $1 < r < 10$ μm) detected by MIP analysis, in which the family of smaller pores saturates before the family of larger pores [70]. The water amount absorbed by capillarity was highest in samples CA-Al-6 and CA-R-7 while samples CA-R-1 and CA-B1-2 absorbed the least amount of water. Capillarity water uptake was fastest in samples CA-M2-1, CA-B1-2, CA-B1-4, CA-B2-3 and CA-AL-6, which showed a higher capillarity coefficient (C_C) (>0.025 g/cm^2 min$^{0.5}$), while samples CA-R-1 and CA-R-9 displayed the slowest values (<0.015 g/cm^2 min$^{0.5}$) (Table 4). Microcracks in samples CA-M2-1 CA-AL-6 and CA-B2-3 (Fig. 3h) could have favoured the capillarity water uptake.

Open porosity values from the hydric tests (P_H) were highest in samples CA-B1-4 and CA-R-7 (44.33% and 42.17%, respectively) and lowest in the south-west filling mortars (sample CA-R-1 with 29.17% and sample CA-R-9 with 29.11%). Considering the higher P_H values of the samples from each structure (Table 4), the highest P_H values were obtained for mortars from the south-east medieval wall and bastions (samples CA-M2-1, CA-B1-2, CA-B1-4 and CA-B2-1), south-west filling mortars (samples CA-R-7 and CA-R-8) and mortar from the lunette vault (sample CA-AL-2).

The largest amount of water was absorbed by the samples with the highest P_H values (Table 4 and Fig. 6a). Samples CA-M2-1, CA-B1-4, CA-R-7, CA-R-8 and CA-Al-2 showed the highest values (>20%) of free water absorption (A_b) and forced water absorption (A_f) and were the fastest absorbing the water (high C_a values in

Table 4
Hydric parameters and porosity values of the lime mortars from Amaiur Castle. A_b: Free water absorption (%). A_f: forced water absorption (%). A_x: degree of pore interconnection (%). S: Saturation coefficient (%). Ca: absorption coefficient (g/min$^{0.5}$). D_i: drying index. ρH_b: bulk density (g/cm^3). ρH_{sk}: skeletal density (g/cm^3). C_c: capillarity coefficient (g/cm^2 min$^{0.5}$). H_c: Height of the water level during capillary uptake (mm s$^{-0.5}$). P_{HT} and P_{MIP}: open porosity (%) determined by hydric tests (HT) and mercury intrusion porosimetry (MIP), respectively.

	CA-M2-1	CA-M2-3	CA-AL-2	CA-AL-6	CA-R-1	CA-R-7	CA-R-8	CA-R-9	CA-B1-2	CA-B1-4	CA-B1-11	CA-B1-13	CA-B2-1	CA-B2-3
A_b	24.10	19.38	20.40	18.90	15.80	29.58	22.63	15.18	18.61	31.59	16.49	16.34	17.99	17.58
A_f	25.05	20.04	20.96	19.24	16.30	31.54	25.22	16.28	19.27	33.13	19.59	17.98	22.60	17.75
A_x	3.81	3.30	2.67	1.76	3.06	6.22	10.28	6.75	3.40	4.65	15.85	9.11	20.41	1.00
S	91.95	93.40	94.46	96.92	96.37	90.25	87.76	92.16	91.84	91.16	72.91	90.65	78.78	96.00
C_a	12.05	9.69	10.20	9.45	7.90	14.79	11.32	7.59	9.31	15.79	8.24	8.17	8.99	8.79
D_i	0.246	0.249	0.248	0.249	0.251	0.244	0.247	0.251	0.249	0.240	0.248	0.249	0.247	0.249
ρ_{Hb}	1.57	1.68	1.68	1.73	1.79	1.34	1.52	1.79	1.72	1.34	1.63	1.64	1.49	1.72
ρ_{Hsk}	2.59	2.54	2.59	2.59	2.53	2.31	2.47	2.52	2.58	2.40	2.39	2.33	2.26	2.48
C_c	0.040	0.024	0.022	0.030	0.010	0.023	0.021	0.014	0.028	0.028	0.022	0.020	0.017	0.029
H_c	0.81	0.65	0.65	0.65	0.58	0.65	0.97	0.65	0.78	0.97	1.16	0.97	1.03	1.18
P_{TH}	39.3	33.8	35.1	33.3	29.2	42.2	38.4	29.1	33.2	44.3	31.9	29.6	33.8	30.5
P_{MIP}	34.1	31.4	31.6	–	31	–	26.3	–	31	45	–	27.7	29.2	37.8

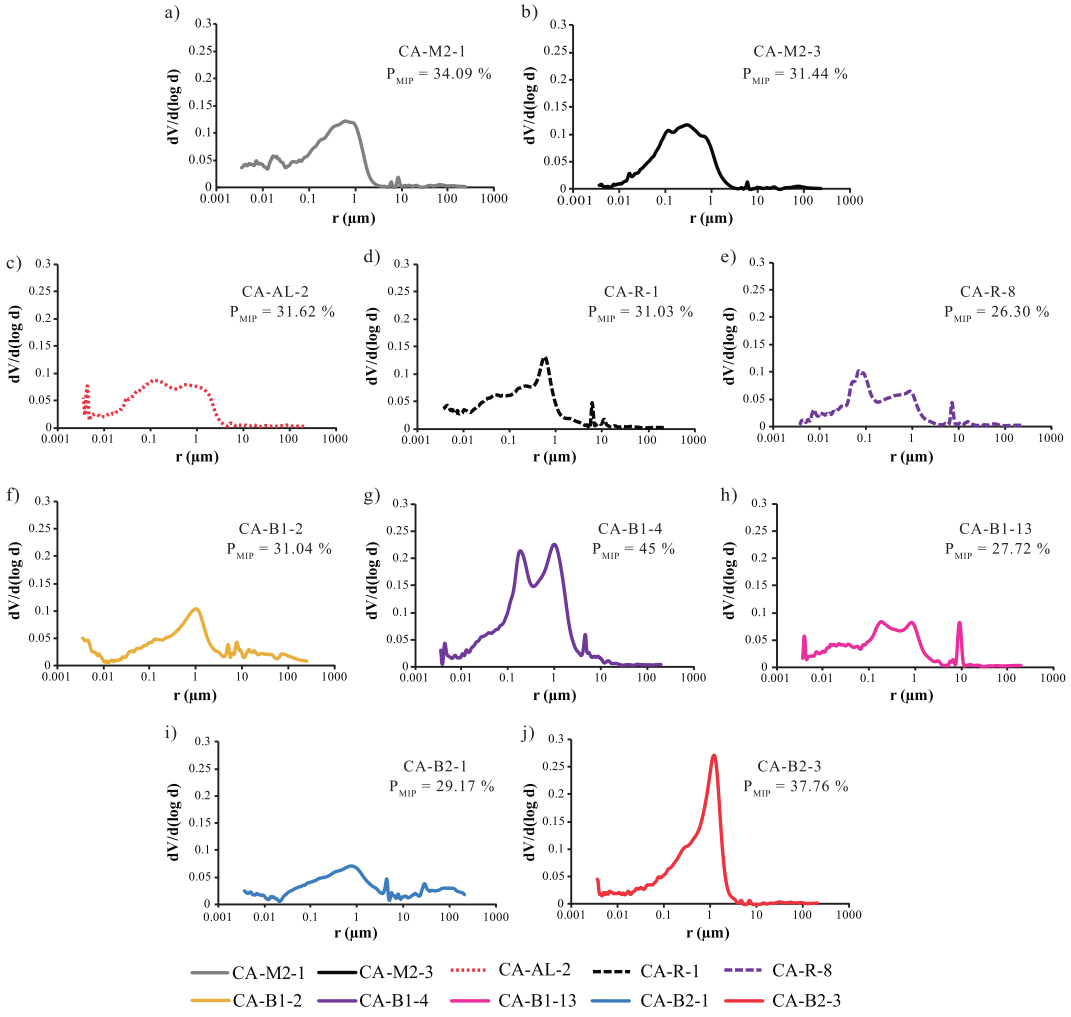

Fig. 5. Pore size distribution curves of lime mortars from Amaiur Castle obtained by mercury intrusion porosimetry. (a) Sample CA-M2-1, (b) Sample CA-M2-3, (c) Sample CA-AL-2, (d) Sample CA-R-1, (e) Sample CA-R-8, (f) Sample CA-B1-2, (g) Sample CA-B1-4, (h) Sample CA-B1-13, (i) Sample CA-B2-1, (j) Sample CA-B2-3. Accessible pore radius (in µm) *vs.* incremental pore volume (in cm^3/g) is represented.

Table 4). Sample CA-B2-1 also absorbed a large amount of water by forced absorption.

The P_H values were similar to the values obtained by MIP (P_{MIP}). Nevertheless, the slight differences between them are caused by the two different fluids used and the different exerted pressures (water at atmospheric pressure in the HT and mercury at 414 MPa in MIP analysis). Samples with the highest open porosity values show the greatest difference

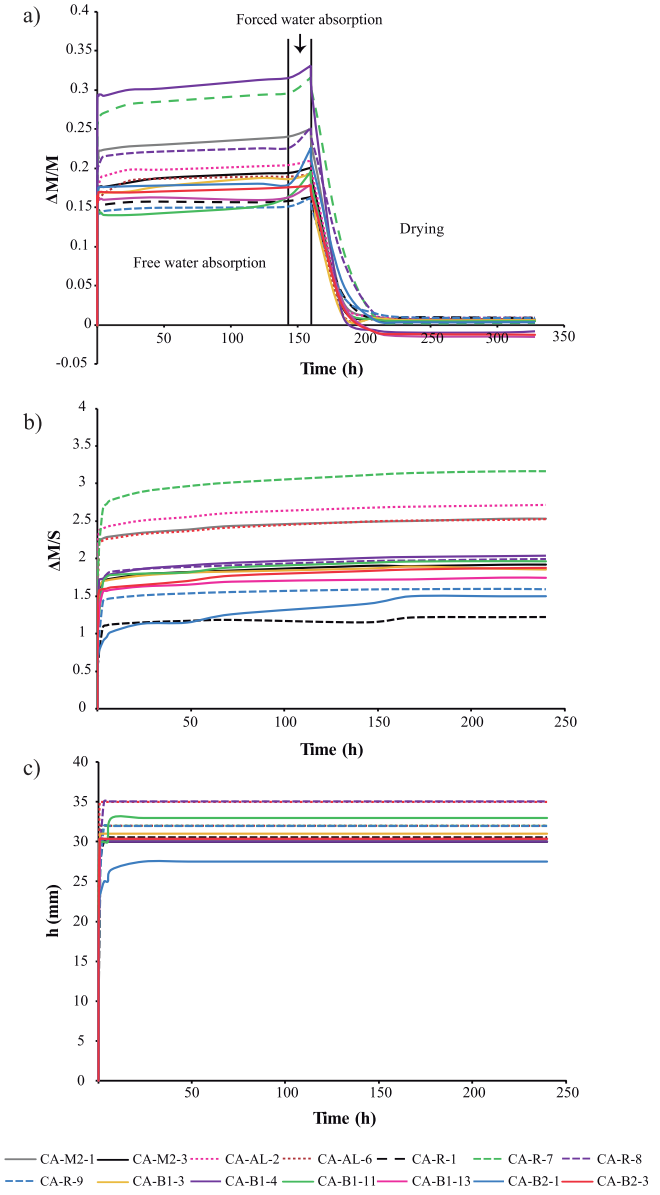

Fig. 6. Hydric behaviour of the lime mortars from Amaiur Castle. (a) Free water absorption, forced water absorption and drying curves. Weight variation (ΔM/M) versus time (in hours). (b) Capillarity curves: Weight variation (ΔM/S) versus time (in hours) and (c) capillarity front curves. Height (in mm) versus time (in hours).

between skeletal and bulk densities (ρHsk and ρHb, respectively) (Table 4).

When the samples from each different structure are compared, the high porosity, high water absorption capacity and poor pore interconnection (high A_x) of samples CA-M2-1, CA-AL-2, CA-R-7, CA-R-8 and CA-B2-1 favour mortar decay since their tortuous pore system hinders the water flow outward. Although sample CA-B1-4 dries the fastest (low D_i), its high porosity and water absorption capacity could also affect its durability. Sample CA-AL-6 is more susceptible to deterioration by capillarity since it not only absorbs a greater amount of water by capillarity but also uptakes the water faster. Furthermore, samples CA-B1-11 and CA-B1-13 took longer to dry (high D_i) and show poor pore interconnection (high A_x), which leads to water retention inside for longer, favouring mortar decay.

4.3. Ultrasonic pulse velocity test

Table 5 summarizes values of the propagation velocity of P waves (V_p) and structural anisotropy (ΔM).

P-wave velocity may vary according to the mineralogy, texture and porosity of the material [15,72]. All studied samples show the same mineralogy with slight variations; thus, the texture and porosity will be the main factors that affect the V_p values. However, the variation in the velocity of the P waves is not due to the size of the aggregates, but rather the increase in velocity is due to the high content of calcareous aggregates. [73–75]. The higher V_p values were measured in samples with a larger amount of aggregates (samples CA-R-1 and CA-R-9, corresponding to filling mortars from the SE area), whereas the lower values were obtained in the mortars with the lowest aggregate content (samples CA-AL-2 and CA-AL-6 from the cistern) (Fig. 2 g-h and i, respectively). Propagation velocity of ultrasonic pulses is also affected by the porosity, with the V_p value decreasing with higher porosity [17,75]. Accordingly, the lowest V_p values were detected in the samples with the highest porosity values, as measured in MIP analysis and hydric tests (Table 4) and observed in the petrographic study (Fig. 4c and d). Besides, the small-scale anisotropies within the material such as microcracks not only affect water circulation but also decrease the V_p values [76,77]. Thus, the high frequency of microcracks in sample CA-M2-1 (Fig. 4h) could explain the lowest V_p value measured in this sample (Table 5). Structural anisotropy (ΔM) confirms the heterogeneous mortar texture of all mortars. The large size of aggregates in the south-west filling mortar samples (samples CA-R-7 and CA-R-8) explains the high ΔM values.

4.4. Colorimetry

Chromatic parameters of each mortar sample are summarised in Table 6. The lightness (L*) values around 80 and the values measured for the chromatic axes (a* and b*) indicated samples with a tendency toward the light grey field. The lower L* values were measured in samples CA-AL-6, CA-R-8, CA-B1-4, CA-B2-1 and CA-B2-3. The a* and b* values are similar in all samples, although sample CA-M2-1, samples from the cistern (CA-AL-2, CA-AL-6) and from the 17th century bastion (CA-B2-1 and CA-B2-3) show higher values. The high chromatic axes values and the low L* values of samples from the 17th century bastion is explained by the presence of ceramic fragments in the mortar.

Table 5
Results of the ultrasonic pulse velocity test in the lime mortars from Amaiur Castle. V_{P1}, V_{P2} and V_{P3}: P-wave velocity in the three orthogonal directions (in m/s). ΔV_p: Average value of the P-wave velocities. σV_p: standard deviation. ΔM: structural anisotropy (%).

	CA-M2-1	CA-M2-3	CA-AL-2	CA-AL-6	CA-R-1	CA-R-7	CA-R-8	CA-R-9	CA-B1-2	CA-B1-4	CA-B1-11	CA-B1-13	CA-B2-1	CA-B2-3
V_{P1}	157.61	237.70	188.17	190.22	279.28	225.16	257.58	271.60	244.27	213.06	233.90	239.13	223.77	210.42
V_{P2}	160.40	244.09	204.82	211.18	295.77	253.73	277.31	285.09	248.06	224.49	250.03	253.77	229.39	216.81
V_{P3}	170.27	250	193.18	193.71	290.18	230.26	272.73	277.31	264.46	215,95	235.49	239.90	244.19	219.03
ΔV_p	162.76	243.93	195.39	198.37	288.41	236.38	269.21	278	252.26	217.83	239.81	244.27	232.45	215.42
σVp	6.65	6.15	8.54	11.23	8.39	15.24	10.33	6.77	10.73	5.94	8.87	8.24	10.54	4.47
ΔM	4.67	3.78	5.44	6.04	4.67	6.95	6.34	3.42	4.68	3.25	3.64	3.12	5.49	3.44

Table 6
Chromatic parameters of historic lime mortar samples from Amaiur Castle. L*: Lightness, a* and b*: chromatic coordinates, C*: chroma, H: hue angle.

	CA-M2-1	CA-M2-3	CA-AL-2	CA-AL-6	CA-R-1	CA-R-7	CA-R-8	CA-R-9	CA-B1-2	CA-B1-4	CA-B1-11	CA-B1-13	CA-B2-1	CA-B2-3
L*	80.70	83.60	82.05	77.41	80.10	85.19	77.92	80.83	81.02	84.37	83.14	79.24	79.42	73.70
a*	2.75	1.70	1.806	2.00	1.46	2.05	1.81	1.32	2.00	1.47	2.18	2.52	2.49	3.89
b*	12.06	8.76	10.76	10.94	7.87	9.02	8.37	8.76	9.99	7.76	9.77	9.56	10.44	13.99
C*	12.37	8.93	10.91	11.13	8.00	9.26	8.56	8.86	10.19	7.90	10.02	9.89	10.73	14.52
H	77.25	79.10	80.48	79.63	79.63	77.04	77.83	81.49	78.62	79.20	77.45	75.22	76.59	74.46

5. Conclusions

Mortars from Amaiur Castle were prepared with the hot-mixing method, most likely using an impure limestone or dolostone as raw material for the manufacturing of lime and angular carbonated aggregates, both of which induced high mechanical strength and cohesion in the hardened mortars. The use of hot lime mortars certainly implies an advantage due to their ease of manufacture in cold climates. At the same time, high durability is expected in hot lime mortars under the particular climatic conditions Amaiur Castle is exposed to. Despite this, most of the mortars show microcracks that must be related to their continuous exposure to the thermal variations in the area, with high humidity, abundant precipitation and annual average temperatures of around 13 °C, but which range from a minimum temperature of −19 °C to a maximum of 41 °C. It is likely that these climatic conditions have led to freezing-thawing phenomena within the mortar pores, leading to mortar cracking due to the mechanical stresses produced.

More specifically, the micro-fractured mortars from the south-east 14th-15th century wall and mortars from the south-west 16th century bastion and the south-east 17th century diamond-shaped structure, which show a poorly interconnected pore system, are more susceptible to decay. Additionally, within the filling, mortars in the south-west area are more susceptible to deterioration than those in the south-east area because they show higher porosity and water absorption capacity, poor interconnection among pores and slower drying.

The fact that sample CA-B1-4 shows different hydric parameters and porosity values from the rest of mortars in the south-east 16th century bastion structure might be related to its application as repair mortar, as described in the written sources. Other differences found in the textural (e.g., aggregate size) and physical features of some mortars; for example, between the filling mortar in the south-west and south-east areas, confirm that the walls were filled in two different periods during the remodelling of the castle defences in the 16th and 17th centuries.

CRediT authorship contribution statement

Graciela Ponce-Antón: Conceptualization, Data curation, Writing - original draft. **Anna Arizzi:** Conceptualization. **Giuseppe Cultrone:** Conceptualization. **Maria Cruz Zuluaga:** Conceptualization. **Luis Angel Ortega:** Conceptualization, Funding acquisition. **Juantxo Agirre Mauleon:** Funding acquisition.

Declaration of Competing Interest

The authors declare that they have no known competing financial interests or personal relationships that could have appeared to influence the work reported in this paper.

Acknowledgments

This study was supported by the IT1193-19 Research Group of the Basque Government and the Junta de Andalucía Research Group RNM179 and Research Project MAT2016-75889-R. G.P.-A. acknowledges the PhD research grant of the Basque Government [2015-1-02-35]. The authors would also like to thank Peter Smith for reviewing the use of English in the manuscript.

References

[1] W. Wallace, On ancient mortars, Chem. News 11 (1865) 185–186.
[2] Venice, Charter, International Charter for the Conservation and Restoration of Monuments and Sites. Available online: http://icomos.org/charters/venice_e.pdf (accessed on 27 March 2020). (1964).
[3] ICOMOS, Declaration of Amsterdam. Available online: https://www.icomos.org/en/and/169-thedeclaration-of-amsterdam (accessed on 10 January 2020). (1975).
[4] C. Groot, G.J. Ashall, J.J. Hughes, P.J. Bartos, Characterisation of old mortars with respect to their repair: a state of the art, Rilem Rep. 28 (2007) 1.
[5] L. Schueremans, Ö. Cizer, E. Janssens, G. Serré, K.V. Balen, Characterization of repair mortars for the assessment of their compatibility in restoration projects: research and practice, Constr. Build. Mater. 25 (12) (2011) 4338–4350.
[6] J.J. Hughes, S.J. Cuthbert, The petrography and microstructure of medieval lime mortars from the west of Scotland: implications for the formulation of repair and replacement mortars, Mater. Struct. 33 (9) (2000) 594–600.
[7] I. Papayianni, V. Pachta, M. Stefanidou, Analysis of ancient mortars and design of compatible repair mortars: the case study of Odeion of the archaeological site of Dion, Constr. Build. Mater. 40 (2013) 84–92.
[8] H. Morillas, P. Vazquez, M. Maguregui, I. Marcaida, L.F.O. Silva, Composition and porosity study of original and restoration materials included in a coastal historical construction, Constr. Build. Mater. 178 (2018) 384–392.
[9] G. Borsoi, A.S. Silva, P. Menezes, A. Candeias, J. Mirão, Analytical characterization of ancient mortars from the archaeological roman site of Pisões (Beja, Portugal), Constr. Build. Mater. 204 (2019) 597–608.
[10] G. Ponce-Antón, A. Arizzi, M.C. Zuluaga, G. Cultrone, L.A. Ortega, J. Agirre Mauleon, Mineralogical, textural and physical characterisation to determine deterioration susceptibility of Irulegi castle lime mortars (Navarre, Spain), Materials 12 (4) (2019) 584.
[11] M. Thomson, J.E. Lindqvist, J. Elsen, C.J.W.P. Groot, 2.5. Porosity of mortars, in: C. Groot, G. Ashall, J. Hughes (Eds.) Characterisation of Old Mortars with Respect to their Repair-State of the Art. Report of RILEM Technical Committee 167-COM, 2007, pp. 77-106.
[12] N.S. Martys, C.F. Ferraris, Capillary transport in mortars and concrete, Cem. Concr. Res. 27 (5) (1997) 747–760.
[13] R.P.J. van Hees, L. Binda, I. Papayianni, E. Toumbakari, Characterisation and damage analysis of old mortars, Mater. Struct. 37 (9) (2004) 644–648.
[14] P. Whiteley, H.D. Russman, T.D. Bishop, Porosity of building materials-a collection of published results, J. Oil Colour Chem. Assoc. 60 (4) (1977) 142–150.
[15] G. Cultrone, A. Luque, E. Sebastián, Petrophysical and durability tests on sedimentary stones to evaluate their quality as building materials, Q. J. Eng. Geol. Hydrogeol. 45 (4) (2012) 415–422.
[16] C. Borges, A. Santos Silva, R. Veiga, Durability of ancient lime mortars in humid environment, Constr. Build. Mater. 66 (2014) 606–620.
[17] A. Arizzi, G. Martinez-Huerga, E. Sebastián-Pardo, G. Cultrone, Mineralogical, textural and physical-mechanical study of hydraulic lime mortars cured under different moisture conditions, Mater. Constr. 65 (318) (2015) e053, https://doi.org/10.3989/mc.2015.v65.i31810.3989/mc.2015.03514.
[18] O.M. Essenwanger, General Climatology 1C: Classification of Climates, Elsevier Science, Amsterdam; London, 2001.
[19] P. Brimblecombe, Heritage climatology, in: R.A. Lefebre, C. Sabbioni (Eds.), Climate and cultural heritage Edipuglia, Bari, Italy, 2010, pp. 54–57.
[20] B. Menéndez, Estimators of the impact of climate change in salt weathering of cultural heritage, Geosciences 8 (11) (2018) 401.
[21] M.C. Peel, B.L. Finlayson, T.A. McMahon, Updated world map of the Köppen-Geiger climate classification, Hydrol. Earth Syst. Sci. 11 (5) (2007) 1633–1644.
[22] AEMET, Iberian Climate Atlas, Agencia Estatal de Meteorología (España) and Instituto de Meteorología (Portugal), Madrid, Spain, 2011.
[23] Arizkun. Available on line: http://meteo.navarra.es/climatologia/selfichaclima.cfm?IDEstacion=66&tipo=MAN (accesed on 23 January 2020). (Accessed accessed on 23 January 2020.
[24] Gorramendi. Available online: http://meteo.navarra.es/climatologia/fichasclimaticasaut_estacion.cfm?IDestacion=25 (accessed on 23 January 2020). (Accessed 23 January 2020.

[25] D. Langmuir, Aqueous Environmental Geochemistry, Prentice Hall, Upper Saddle River, NJ, 1997.
[26] George W Scherer, Crystallization in pores, Cem. Concr. Res. 29 (8) (1999) 1347–1358.
[27] O Coussy, Deformation and stress from in-pore drying-induced crystallization of salt, J. Mech. Phys. Solids 54 (8) (2006) 1517–1547.
[28] G. Ponce-Antón, M.C. Zuluaga, L.A. Ortega, J.A. Mauleon, Multi-analytical approach for chemical-mineralogical characterization of reaction rims in the lime mortars from Amaiur Castle (Navarre, Spain), Microchem. J. 152 (2020) 104303.
[29] A. Henry, J. Stewart, Practical building conservation: Mortars, renders & plasters, Practical Building Conservation. English Heritage, Surrey 2011.
[30] N. Copsey, Hot Mixed Lime and Traditional Mortars: A Practical Guide to Their Use in Conservation and Repair, The Crowood Press, Ramsbury, Marlborough, 2019.
[31] A. Forster, Hot-lime mortars: a current perspective, J. Archit. Conserv. 10 (3) (2004) 7–27.
[32] J. Válek, T. Matas, Experimental Study of Hot Mixed Mortars in Comparison with Lime Putty and Hydrate Mortars, Historic Mortars, Springer Netherlands, Dordrecht, 2012, pp. 269-281.
[33] I. Sagredo, Navarra. Castillos que defendieron el reino (Tomo I) de Laguardia a Foix, y del Moncayo al Goierri, Pamiela Ed., Pamplona, 2006.
[34] I. Sagredo, El castillo de Amaiur a través de la historia de Navarra, Pamiela Ed., Pamplona, 2009.
[35] AGN, Royal and General Archive of Navarre, Rena Papers, Box 33080, 1517.
[36] AGN, Royal and General Archive of Navarre, Rena Papers, Box 27, N.14, 1521.
[37] G. Ponce-Antón, M.C. Zuluaga, L.A. Ortega, J.A. Mauleon, Petrographic and chemical-mineralogical characterization of mortars from the cistern at Amaiur castle (Navarre, Spain) Minerals, 10 (4), (2020) 311.
[38] R.L. Folk, A comparison chart for visual percentage estimation, J. Sediment. Res. 21 (1) (1951) 32–33.
[39] UNE-EN 13755 Natural stone test methods determination of water absorption at atmospheric pressure, 2008, AENOR, Madrid.
[40] G. Cultrone, M.J. De La Torre, E. Sebastián, O. Cazalla, Evaluation of bricks durability using destructive and nondestructive methods (DT and NDT), Mater. Constr. 53 (269) (2003) 41–59.
[41] RILEM, Recommended test to measure the deterioration of stone and to assess the differences of treatment methods, Mater. Struct. 13 1980 175-253.
[42] UNE-EN 1936, Natural stone test methods. Determination of real density and apparent density, and of total and open porosity, 2007, AENOR, Madrid.
[43] NORMAL 29/88, Misura dell'indice di asciugamento (drying index), 1988., CNR-ICR, Rome.
[44] UNE-EN 1925, Natural stone test methods. Determination of water absorptioncoefficient by capillarity, 2000, AENOR, Madrid.
[45] V.M. Malhotra, N.J. Carino, Handbook on nondestructive testing of concrete, 2004.
[46] ASTM D 2845–05, Standard Method for Laboratory Determination of Pulse Velocities and Ultrasonic Elastic Constants of Rock, ASTM International Standards Worldwide, Pennsylvania, 2005.
[47] J. Guyader, A. Denis, Wave propagation in anisotropic rocks under stress evaluation of the quality of slates, Bull. Int. Assoc. Eng. Geol. 33 (1) (1986) 49–55.
[48] A. López, G.A. Guzmán, A.R. Di Sarli, Color stability in mortars and concretes. Part 1: study on architectural mortars, Constr. Build. Mater. 120 (2016) 617–622.
[49] UNE-EN 15886, Conservation of cultural property. Test methods. Colour measurement of surfaces, 2011, AENOR, Madrid.
[50] G. Ponce-Antón, L.A. Ortega, M.C. Zuluaga, A. Alonso-Olazabal, J.L. Solaun, Hydrotalcite and hydrocalumite in mortar binders from the medieval castle of portilla (Álava, North Spain): accurate mineralogical control to achieve more reliable chronological ages, Minerals 8 (8) (2018) 326.
[51] A. Arizzi, G. Cultrone, The difference in behaviour between calcitic and dolomitic lime mortars set under dry conditions: The relationship between textural and physical–mechanical properties, Cem. Concr. Res. 42 (6) (2012) 818–826.
[52] A. Diekamp, J. Konzett, P.W. Mirwald, Magnesian lime mortars–Identification of magnesium phases in medieval mortars and plasters with imaging techniques, 12th Euroseminar on Microscopy Applied to Building Materials, Dortmund, Germany, 2009, pp. 15-19.
[53] L. Chever, S. Pavía, R. Howard, Physical properties of magnesian lime mortars, Mater. Struct. 43 (2010) 283–296.
[54] A.R. Santos, M. do Rosário Veiga, A.S. Silva, J. de Brito, J.I. Álvarez, Evolution of the microstructure of lime based mortars and influence on the mechanical behaviour: the role of the aggregates, Constr. Build. Mater. 187 (2018) 907–922.
[55] J. Lanas, J.I. Alvarez-Galindo, Masonry repair lime-based mortars: factors affecting the mechanical behavior, Cem. Concr. Res. 33 (11) (2003) 1867–1876.
[56] G. Cultrone, E. Sebastian, M.O. Huertas, Durability of masonry systems: a laboratory study, Constr. Build. Mater. 21 (1) (2007) 40–51.
[57] A. Arizzi, J. Martínez Martínez, G. Cultrone, D. Benavente, Mechanical evolution of lime mortars during the carbonation process, Key Eng. Mater. Trans. Tech. Publ. 465 (2011) 483–486.
[58] A. Arizzi, G. Cultrone, The influence of aggregate texture, morphology and grading on the carbonation of non-hydraulic (aerial) lime-based mortars, Q. J. Eng. Geol. Hydrogeol. 46 (4) (2013) 507–520.
[59] M. Stefanidou, I. Papayianni, The role of aggregates on the structure and properties of lime mortars, Cem. Concr. Compos. 27 (9-10) (2005) 914–919.
[60] E. Galán Pérez, A. García de Domingo, A. Cabra Gil, J. Ganzález Lastra, L.M. Matinez Torres, A. Pesquera Pérez, Memoria Hoja 66-III (Maya de Baztán). Mapa Geológico de Navarra. E. 1:25000, Diputación Foral de Navarra2002.
[61] D. Juch, H.F. Krausse, D. Müller, H. Requadt, D. Schafer, J. Sole, L. Villalobos, Memoria Hoja 66 (Maya del Baztan). Mapa Geológico de España E. 1:50.000. Segunda Serie (MAGNA), Primera edición ed.1974.
[62] M. Back, M. Bauer, H. Stanjek, S. Peiffer, Sequestration of CO_2 after reaction with alkaline earth metal oxides CaO and MgO, Appl. Geochem. 26 (7) (2011) 1097–1107.
[63] R.M. Dheilly, A. Bouguerra, B. Beaudoin, J. Tudo, M. Queneudec, Hydromagnesite development in magnesian lime mortars, Mater. Sci. Eng., A 268 (1-2) (1999) 127–131.
[64] M. Zajac, S.K. Bremseth, M. Whitehead, M. Ben Haha, Effect of $CaMg(CO_3)_2$ on hydrate assemblages and mechanical properties of hydrated cement pastes at 40°C and 60°C, Cem. Concr. Res. 65 (2014) 21–29.
[65] A. Machner, M. Zajac, M. Ben Haha, K.O. Kjellsen, M.R. Geiker, K. De Weerdt, Limitations of the hydrotalcite formation in Portland composite cement pastes containing dolomite and metakaolin, Cem. Concr. Res. 105 (2018) 1–17.
[66] J. Lanas, J.I. Alvarez, Dolomitic limes: evolution of the slaking process under different conditions, Thermochim. Acta 423 (1–2) (2004) 1–12.
[67] M. Arandigoyen, J.P. Bernal, M.B. López, J.I. Alvarez, Lime-pastes with different kneading water: pore structure and capillary porosity, Appl. Surf. Sci. 252 (5) (2005) 1449–1459.
[68] R.M. Lawrence, T.J. Mays, S.P. Rigby, P. Walker, D. D'Ayala, Effects of carbonation on the pore structure of non-hydraulic lime mortars, Cem. Concr. Res. 37 (7) (2007) 1059–1069.
[69] G.W. Scherer, Theory of drying, J. Am. Ceram. Soc. 73 (1) (1990) 3–14.
[70] K. Beck, M. Al-Mukhtar, O. Rozenbaum, M. Rautureau, Characterization, water transfer properties and deterioration in tuffeau: building material in the Loire valley-France, Build. Environ. 38 (9) (2003) 1151–1162.
[71] A. Arizzi, G. Cultrone, The water transfer properties and drying shrinkage of aerial lime-based mortars: An assessment of their quality as repair rendering materials, Environ. Earth Sci. 71 (4) (2014) 1699–1710.
[72] J.H. Schön, Physical properties of rocks: fundamentals and principles of petrophysics. Handbook of geophysical exploration. Section I, Seismic exploration, Pergamon, Oxford, 1996.
[73] D.G. Aggelis, T.P. Philippidis, Ultrasonic wave dispersion and attenuation in fresh mortar, NDT E Int. 37 (8) (2004) 617–631.
[74] T.P. Philippidis, D.G. Aggelis, Experimental study of wave dispersion and attenuation in concrete, Ultrasonics 43 (7) (2005) 584–595.
[75] A. Arizzi, J. Martínez-Martínez, G. Cultrone, Ultrasonic wave propagation through lime mortars: An alternative and non-destructive tool for textural characterization, Mater. Struct./Mater. Constr. 46 (8) (2013) 1321–1335.
[76] C. Hall, W.D. Hoff, Water Transport in Brick, Stone and Concrete, Taylor & Francis, London, 2002.
[77] D. Benavente, J. Martínez-Martínez, P. Jáuregui, M.A. Rodrıguez, M.G. del Cura, Assessment of the strength of building rocks using signal processing procedures, Constr. Build. Mater. 20 (8) (2006) 562–568.